Contrib Mineral Petrol
DOI 10.1007/s00410-012-0726-8

ORIGINAL PAPER

Metamorphic reaction rate controlled by fluid pressure not confining pressure: implications of dehydration experiments with gypsum

Sergio Llana-Fúnez · John Wheeler · D. R. Faulkner

Received: 1 July 2011 / Accepted: 3 February 2012

Abstract Pressure is a key control on the progress of metamorphic reactions. When fluids are present in rocks, the fluid pressure is commonly different to the load supported by the solid framework. Here, we show experimentally that, when the two pressures are varied independently, fluid pressure exerts the dominant control on reaction rate, even when the rock is compacting. We present 35 experiments on gypsum dehydration with independently controlled confining pressure, pore fluid pressure and temperature. Results show that a pore fluid pressure decrease at constant confining pressure has a strong effect on the average rate of the reaction. A decrease in confining pressure at constant pore fluid pressure has relatively little effect. Our results have implications for reaction kinetics: even though the product phase is supporting more and more load as reaction proceeds, that load does not appear to exert a chemical effect. On the large scale, our results imply that changes in fluid pressure will drive or stop the progress of metamorphic reactions. When estimating depth at which a metamorphic devolatilization reaction occurs, knowledge of the pore fluid pressure may be necessary rather than commonly used lithostatic pressure. This is relevant for basin diagenesis, mineralization in hydrothermal systems and chemical evolution after pore fluid pressure is perturbed by earthquakes.

Keywords Devolatilization reaction · Gypsum dehydration · Experimental petrology · Pore fluid pressure · Diagenesis · Mineralization · Post-seismic response

Introduction

The fundamental concept of equilibrium in devolatilization reactions is based on the premise that the pressure of the fluid phase is equal to the pressure of the solid (Fyfe et al. 1978; Rubie and Thompson 1985). Under these circumstances, the equilibrium is pressure-dependent and that is fundamental to our understanding of such reactions. However, in many crustal settings, pore fluid pressure will vary from hydrostatic to lithostatic (Hanshaw and Bredehoeft 1968; Miller et al. 2003), for example basin sediments undergoing compaction, geothermal fields and hydrothermal systems within mid-ocean ridges and around plutons. In places where fluid pressure is equal to lithostatic, sudden events (e.g., earthquakes) will change fluid pressure as porous rock rapidly dilates and compacts. Thus, the more general case in nature for a rock undergoing a metamorphic reaction in the crust is that pore fluid pressure (P_f) is significantly less than the lithostatic or confining pressure (P_c). How, then, are metamorphic reactions influenced by these two independently variable quantities? In this contribution, we address this question using experiments on gypsum in which the fluid and confining pressures are varied independently. The issue is important for understanding metamorphic evolution in a wide variety of

Communicated by J. Blundy.

Electronic supplementary material The online version of this article (doi:10.1007/s00410-012-0726-8) contains supplementary material, which is available to authorized users.

S. Llana-Fúnez · J. Wheeler · D. R. Faulkner
Department of Earth and Ocean Sciences, University of Liverpool, 4 Brownlow Street, Liverpool L69 3GP, UK

S. Llana-Fúnez (✉)
Departamento de Geología, Universidad de Oviedo, Calle Arias de Velasco s/n, 33005 Oviedo, Spain
e-mail: slf@geol.uniovi.es

Published online: 21 February 2012

geological settings, because whilst T and P_c vary slowly through time, much more rapid variations in P_f are to be expected.

Theoretical framework

Stresses

Although the word "pressure" is used for convenience, there is, in fact, a state of anisotropic (non-hydrostatic) stress in the solid when $P_c > P_f$ (Paterson 1973; Dahlen 1992). Figure 1a shows stress trajectories in a model porous rock to emphasize this point, and Fig. 1b shows the differential stress: stress is both anisotropic and heterogeneous on the grain scale. Provided there is sufficient pore connectivity, pore fluid pressure will be uniform; force balance dictates that the normal stress in the solid at solid–fluid contacts must be equal to that pressure. Along solid–solid contacts, stress may have different values on each side, although force balance provides some constraints. For simplicity, we have assumed no shear stress along boundaries in the construction of Fig. 1 (this is why stress trajectories are parallel and perpendicular to boundaries), though it is not known to what extent grain boundaries can support shear stress. Along solid–solid contacts, normal stress will be of the order of P_c, since it must—on average—support the rock load, but in detail, it may vary from point to point and will depend on contact area between grains. If porosity is substantial, then the average normal stress along solid–solid contacts, which we write here as σ_s, will be greater than P_c. The details of how heterogeneous stresses in porous media are analysed are beyond the scope of this contribution (see e.g., Bear and Bachmat 1991).

Chemistry: our conceptual model

Our arguments in this section are quite general but are illustrated with respect to gypsum dehydration. The stable dehydration product at 1 bar is anhydrite, but in our experiments bassanite forms. This is clearly metastable as shown by, for example, its higher solubility relative to anhydrite (e.g., Fig. 4 of Partridge and White 1929). Bassanite has a stability field above 235 MPa (Mirwald 2008), but our experiments are at lower pressures than that. In the context of this contribution, the key point is that there is *no* evidence for anhydrite formation in our experiments—for example, we would have detected it by EBSD in the microstructural work we have already undertaken (Hildyard et al. 2011). We infer that anhydrite cannot nucleate and bassanite nucleates and grows metastably. The phase changes are driven by chemical potential differences between gypsum and bassanite, and the properties of anhydrite are irrelevant. Our model and conclusions are not compromised by the metastability of bassanite.

Under the conditions of the experiment in excess of water and at elevated water pressure, gypsum breaks down to bassanite in a pressure-dependent reaction.

$$CaSO_4 \cdot 2H_2O = CaSO_4 \cdot 0.5H_2O + 1.5H_2O \quad (1)$$

Figure 1a shows possible pathways for transport of Ca^{2+} and SO_4^{2-} ions. Path 1 is entirely within pore fluid. Path 2 involves transport *across* a gypsum/bassanite interface (with H_2O being lost along a separate pathway, not shown). Path 3 involves dissolution of gypsum in a pore, followed by transport along a bassanite/bassanite grain boundary. Path 4 involves dissolution at a gypsum/gypsum boundary and precipitation of bassanite from pore fluid. In a system

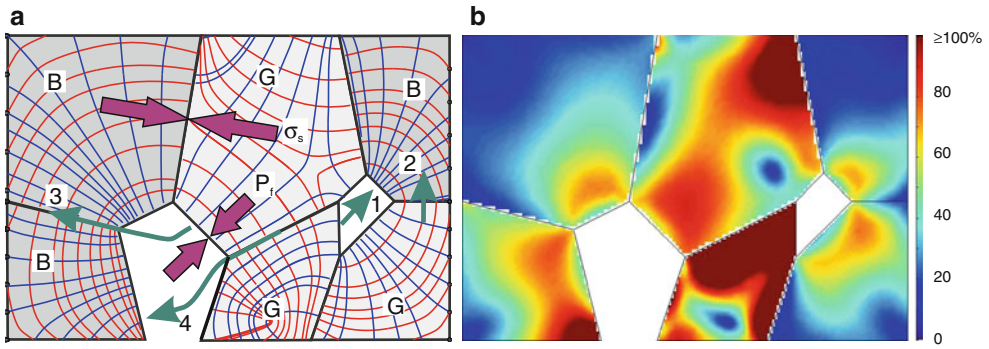

Fig. 1 **a** Heterogeneous stresses in a porous material under effective pressure. *Lines* in *solids* indicate maximum (*red*) and minimum (*blue*) compressive stress trajectories, calculated precisely but based on sketch in Wheeler (1987). *Filled arrows* indicate normal stresses across interfaces: solid–fluid contacts will be at the pressure of the fluids (P_f), whilst solid–solid contacts will have a higher average normal stress (σ_s) depending on the bulk effective pressure and contact area. *G,* gypsum; *B,* bassanite. *Thin arrows* indicate possible transport pathways for Ca^{2+} and SO_4^{2-} ions during reaction; see text for details. **b** Differential stress *colour-coded* as proportion of σ_s–P_f for the stress system in **a**. Note that locally some stresses exceed that value but are not given separate colours here. Differential stresses are of the order of the effective "pressure" P_e

where pressure is everywhere hydrostatic, all four pathways (and any others that can be envisaged) will involve the same Gibbs free energy reduction per mole of product formed.

However, we are considering a stressed system, where the Gibbs free energy is then *undefined*. Theory predicts that *local* chemical potentials can be defined at interfaces as a function of normal stresses (e.g., Paterson 1973). A fundamental relationship is (e.g., Eq. 8 of that work):

$$\mu = F + \sigma_n V, \tag{2}$$

where σ_n is the normal stress across an interface (Pa), F is the molar Helmholtz free energy of the solid (J/mol), V is the molar volume of the solid (m^3/mol) and μ is the chemical potential of the solid material in an adjacent "phase" in which it can dissolve (J/mol). We use the quotation marks because the "phase" is, for a solid–solid boundary, the interface region, which may have a rather complex structure involving pockets of water and narrower regions, possibly with H_2O present but with properties different to those of bulk water. Eq. 2 can be approximated as

$$\mu \cong \mu_0 + \sigma_n V, \tag{3}$$

where μ_0 is the chemical potential at zero pressure. This approximation applies when the stresses in the system are much less than the elastic moduli of the solids involved (e.g., ~45 GPa for gypsum, Stretton et al. 1997), a condition that applies to the upper part of the Earth apart from very locally (e.g., around crack tips). It is immediately apparent that spatial variations in normal stress give rise to spatial variations in chemical potential and hence chemical disequilibrium, even for a single solid phase. Whilst the (spatially varying) chemical potentials provide the motivation for change, the kinetics of diffusion, interface migration and other processes will govern how reactions actually progress (e.g., Lasaga 1997). Each of the four pathways shown in Fig. 1a now involves different chemical potentials for solid reactants and products. For a proper understanding of metamorphism in stressed systems, it is fundamental to understand both the chemical potentials and the kinetics associated with all reaction pathways.

Previous theoretical work

Bruton and Helgeson (1983) considered solid–fluid interfaces, at which the normal stress is equal to fluid pressure and Eq. 3 becomes

$$\mu \cong \mu_0 + P_f V \tag{4}$$

To précis their argument, if a number of solids are in contact with fluid, then Eq. 4 implies that those solids will reach equilibria governed simply by the fluid pressure—the rock pressure plays a negligible role. They say "calculations and experimental determinations of phase equilibria in hydrostatically stressed systems at a specified pressure (P) can also be applied to non-hydrostatically stressed systems in which $P_f = P$" (p. 551) and proceed with calculations on that basis. However, there is only a short discussion, at the very end of that paper, in which they consider the possibility that solid–solid contacts have chemical effects. There is no basis provided by those authors for their assumption that the grain–grain contacts do not affect equilibria (i.e. that they are chemically isolated). Dahlen (1992) makes the same assumption, more explicitly: "The only restriction is that the reaction must occur in a fluid-saturated rock, by means of dissolution of the solid reactants followed by precipitation of the solid-reaction products at the fluid–solid interface". In essence, the assumption is that reaction proceeds by Path 1 (Fig. 1a) or similar. That restrictive assumption, we assert, requires testing. It has been widely adopted in theoretical models (e.g., Ague et al. 1998) and Eq. 1 of Miller et al. (2003), but this usage does not strengthen the assumption itself. In nature, it is clear that the chemical potentials at solid–solid contacts do have an effect: the prime example is pressure solution, which is driven by differences between chemical potentials at different solid–solid interfaces.

When $P_c > P_f$, there is non-zero effective pressure ($P_e = P_c - P_f$). This is a useful quantity for quantifying compaction, and mechanical behaviour in general, but in our view, it has, in itself, no thermodynamic significance. Nowhere on Fig. 1 is any boundary under a normal stress equal to P_e; nowhere will P_e enter into an expression for chemical potential. Our analysis of reaction rate will be based on identifying the relative influences of P_c and P_f.

Previous experiments on dehydration under effective pressure

We now focus on dehydration reactions, since the expulsion of water is a useful indicator of reaction progress in experiments and its measurement is very accessible in the laboratory. Gypsum dehydration will produce porosity, in which some of the product water will be stored (Fig. 2), but with a net volume increase, some water will be expelled (e.g., Ko et al. 1995). In any dehydration experiment, fluid pressure may be controlled at the ends of a sample but it may evolve in a heterogeneous fashion within, depending on the (evolving) permeability of the sample. This must be taken into account when interpreting results. When $P_c > P_f$, there is non-zero effective pressure ($P_e = P_c - P_f$); so, in addition to water expelled due to net volume increase, compaction will enhance fluid expulsion. The coupled processes of reaction, fluid flow and compaction must be unravelled to identify the contribution of each.

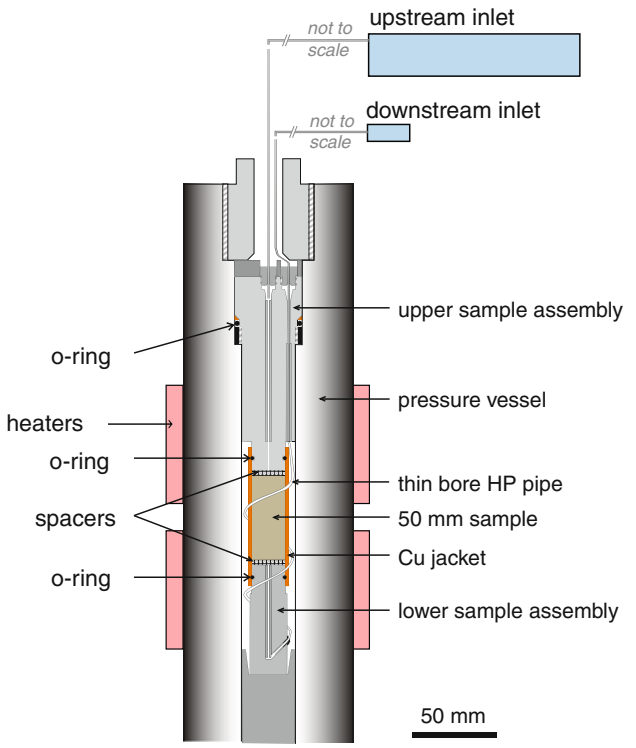

Fig. 2 Arrangement of the sample assembly inside the triaxial cell used in the experiments (based in Mitchell and Faulkner 2008). External band heaters are indicated in *red* colour. The storage capacity of the upstream reservoir is $1.296{\cdot}10^{-14}$ m^3/Pa, 13 times larger that the storage capacity of the downstream reservoir. The actual volume of both reservoirs has not been measured, so the *boxes* in *blue* are not to scale, but the relative volume is shown in the figure to illustrate their difference in size

Ko et al. (1997) monitored fluid expulsion during gypsum dehydration where confining and fluid pressures were different. They show two pairs of experiments in their fig. 8b: high P_f decreases the maximum fluid expulsion rate when T and P_c are kept constant. They infer that high P_f reduces reaction rate, though it could also be argued that high P_f decreases effective stress and hence fluid expelled *by compaction*. Experiments at the same effective stress were compared in an attempt to "cancel out" the effects of compaction. Results from seven experiments at 128°C (their fig. 8c) show that, for the same effective stress, higher P_f was associated with smaller expelled fluid volumes. Again they suggest that this is due to reaction rate. However, there are no rate data explicit in that figure; also, if P_e is fixed, a higher P_f implies a higher P_c so it is unclear whether the contributions of P_f and P_c can readily be distinguished. They concluded that P_f was the relevant pressure to include in a formulation of reaction rate (e.g., Eq. 13b of Wang and Wong 2003).

Llana-Fúnez et al. (2007) studied serpentinite dehydration, again using a volumometer to monitor reaction progress. They inferred that P_f rather than P_c controlled reaction kinetics, though this is shown explicitly by just two pairs of experiments (c58 vs. c18 and c21 vs. c25 on their Fig. 5b). In those experiments, there was no significant compaction.

New work

We present a new dataset of 35 experiments on gypsum dehydration to analyse the relative effects of P_f and P_c on reaction rate, applying best-fit algorithms to volumes of evolved fluid to quantify our approach. We are motivated by the lack of a sound theoretical basis for understanding those effects and by the rather restricted number of experiments that have so far provided relevant information. We use an apparatus in which we control P_f at one end of the sample (where fluid volumes are measured, as in previous studies) but in addition monitor P_f at the other end so as to establish how uniform the fluid pressure is within the sample. This work is part of a larger study on how non-hydrostatic conditions at the grain scale affect the onset and progress of metamorphic reactions. We examine the bulk effect that non-hydrostatic conditions have on the dehydration reaction of polycrystalline gypsum. We selected this system because its behaviour represents the general case where compaction proceeds in parallel with dehydration (Ko et al. 1997).

Experiments and analysis

Apparatus

The experiments were run in a triaxial deformation apparatus using low viscosity oil as confining medium and distilled water as pore fluid (Mitchell and Faulkner 2008), modified so that temperature can be raised and controlled by two external furnaces (Fig. 2). The pore fluid in the specimens is isolated from the confining fluid by a thin-walled copper jacket. Temperature is >80°C in all our experiments. The specimens have 20 mm diameter and approximately 50 mm length. Grooved, pierced end pieces allow pore fluid pressure to be transmitted to the specimen at the top and (optionally) the bottom of the sample cylinders whilst permitting fluid flow to or from the fluid reservoir (Fig. 2). The temperature is monitored at the top of the specimen by a thermocouple providing feedback to the heaters. The temperature gradient between the top and the bottom of the specimen is less than 2°C. A key component of the apparatus is a servo-controlled pore fluid reservoir, where the fluid pressure can be controlled and the fluid volume monitored. At the start of each experiment, temperature was raised whilst both confining and pore fluid pressures were kept sufficiently high, in the stability field

of gypsum, so as to inhibit reaction entirely. The effective pressure at this stage was kept below the target effective pressure of the experiment. Then, pressures were dropped to target values of specific experiments to initiate reaction at a temperature that had already stabilized.

The starting material is Volterra gypsum, a standard material for experimental work in gypsum rocks because of its purity, >95% gypsum (Heard and Rubey 1966; Ko et al. 1995; Olgaard et al. 1995; Stretton 1996; Milsch and Scholz 2005). It has a grain size ranging between 20 and 50 μm, a very low porosity <1% and very low permeability, in the 10^{-16} to 10^{-20} m^2 range, depending on the effective pressure (Milsch et al. 2011). Although overall it is considered a relatively homogeneous rock, locally, it presents a shape and a crystallographic fabric (Hildyard et al. 2009).

Analysis: tracking reaction progress

The dehydration of Volterra gypsum samples in the apparatus, under water pore fluid pressure, produces bassanite (sulphate hemihydrate), a metastable phase in the family of hydrated calcium sulphates (Posjnak 1938; Kelley et al. 1941; Zen 1965; Yamamoto and Kennedy 1969; McConnell et al. 1987; Mirwald 2008). The stable phase, anhydrite, has not been recorded in our experiments: the water volumes expelled are too small, and no anhydrite was found by X-ray diffraction in dehydrated specimens.

Upon heating the samples, the solid loses water and hence weight during reaction. Bassanite has a higher density than gypsum (2.731 against 2.31 g/cm^3), so that unless the solid deforms, porosity develops. If we assume that the solid mass retains its original volume, then 28.7% porosity is calculated for a fully dehydrated specimen. However, under the conditions of our experiments, the volume of water produced is larger than the available pore volume so water will be expelled. For example, at 100°C and 100 MPa ($P_c = P_f$), 37.06% by volume of water is produced, so 8% will be expelled by the end of reaction (Fig. 3). Consequently, expelled water can be used to monitor reaction progress, as done in other hydrated minerals such as serpentine (Llana-Fúnez et al. 2007), but in our case, compaction commonly occurs in parallel with reaction. We could use the final volume of expelled water as a guide to how much compaction has occurred, but is then restricted because some experiments did not dehydrate to completion, and others carried on compacting after dehydration was complete.

All volume expulsion curves show a sigmoidal form as expected from reaction rate theory (Rubie and Thompson 1985; Lasaga 1997). In addition to this, at the early stages of the dehydration, pore connectivity is limited in such low permeability material, affecting the expulsion rate of water

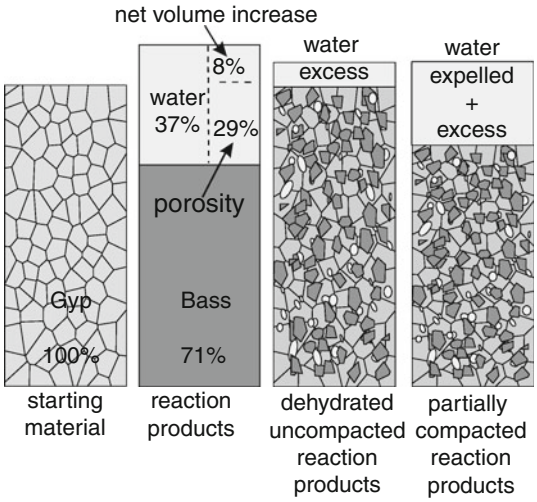

Fig. 3 Sketches showing porosity development and water expelled by reaction and compaction. The excess of water in the specimen during an experiment is measured and used as a proxy for reaction progress and/or compaction

off the dehydrating sites. This produces a transient behaviour that is overcome early in the experiments once reaction generates a threshold porosity draining effectively the sample specimen (Wong et al. 1997; Wang and Wong 2003). In order to compare the reaction rate between experiments in which different amounts of compaction have occurred, we make an empirical correction by dividing the maximum fluid expulsion rate by the actual fluid volume expelled at that time. This is based on the assumption that compaction proceeds in parallel with reaction, and enhances the expulsion rate and fluid volume expelled in proportion. This reaction rate proxy has the additional advantage of bypassing the transient behaviour in the initial stages of the reaction. We define:

$$\text{Reaction rate proxy} = (\text{maximum expulsion rate}) / (\text{volume expelled at that time}) \quad (5)$$

A more complete model for compaction would require a detailed description of the rheology of the porous bassanite-gypsum aggregate, a description which our data can assist with but which will involve a number of additional assumptions. Our empirical reaction rate proxy is sufficient for this contribution because we seek the overall sensitivity of dependence on P_f and P_c.

Analysis: relating reaction progress to pressures

There are two approaches we take. One is to use the free energy change of reaction in a hydrostatic system, calculate this using either P_f or P_c and plot that free energy change against reaction rate proxy. The free energy change as function of temperature *and* pressure has not previously

been published and we derive it in Supplementary Data section. The temperature dependence and equilibrium position for the reaction at 1 bar are given in Kelley et al. (1941). The pressure dependence of the equilibrium has been calculated using molar volumes and compressibilities of solids (Mirwald 2008) and molar volumes of water (Holland and Powell 1998). The free energy of the reaction with respect to temperature and a hydrostatic pressure, $\Delta_r G^o_P$ (J), is,

$$\Delta_r G^o_P = -3591.06 + 529.253T + 0.0775T^2 - 92.705T\ln(T) + 5\cdot10^{-6}P^3 - 5.54\cdot10^{-3}P^2 + 6.8665P, \quad (6)$$

where T is temperature (K) and P is pressure (MPa). Thermodynamic data used and details of free energy calculations leading to equilibrium lines in the background of Figs. 3 and 4 are given in the Supplementary Data section. The Gibbs free energy in a stressed system is not defined, but we calculate it in Eq. 6 with both P_c and P_f as one way to examine their relative effects.

Our second approach makes no detailed reference to thermodynamics. We perform a linear regression on the log of reaction rate proxy as a function of temperature, confining pressure and fluid pressure. This is not to say that we expect a linear relationship, but there is no detailed theoretical framework for specifying the mathematical form of the relationship, and our aim is simply to illustrate the relative sensitivity of rate to the controlling parameters. A rapid increase in reaction rate as a function of T is expected and observed, which is why we use the log of rate.

We could attempt to fit an Arrhenius temperature dependence to reaction rate, but "it is not always appropriate to think of an activation energy for an overall reaction as representing any kind of molecular energy barrier" (Lasaga pp. 61–62). For a reaction such as this, under hydrostatic conditions (with all principal stress components equal), the rate law will involve not just an Arrhenius temperature term but also a term involving reaction affinity (difference in Gibbs free energy between reactants and products) (e.g., Lasaga eqns. 1.193, 2.56). Thus, even in a hydrostatic system, we should not expect an Arrhenius temperature dependence. Our system is more complicated and it is premature to define the quantity that may take the place of affinity in Eq. 6, as the Gibbs free energy is not defined in a system under stress. The strength of our second approach is that it is empirical.

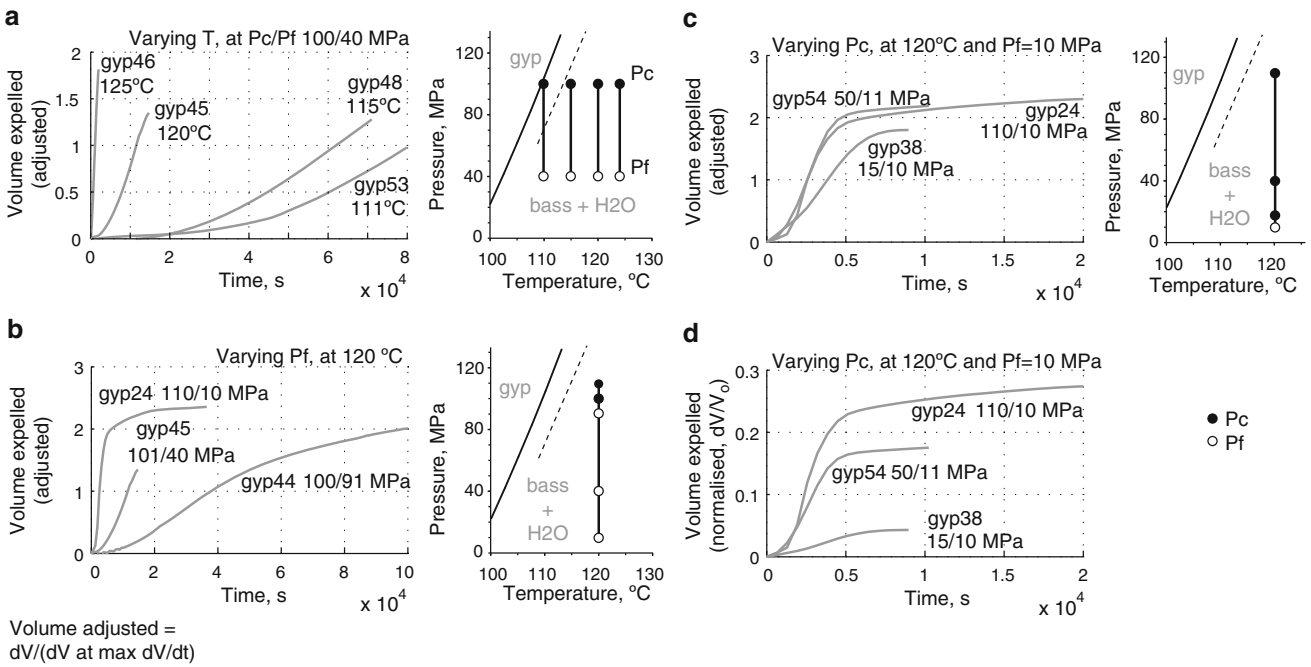

Fig. 4 Sets of dehydration experiments in Volterra gypsum adjusted for compaction: **a** at constant confining (P_c) and pore fluid pressure (P_f) of 100 and 40 MPa, respectively, and increasing temperatures from 111 to 125°C; **b** at constant T of 120°C, 100 MPa confining pressure and increasing pore fluid pressures in separate tests; and **c** at constant T of 120°C, 10 MPa pore fluid pressure and increasing confining pressures in separate tests. Plot in **d** shows the volume of water expelled in the same experiments as in **c** and normalized to sample volume but without the compaction correction. Note that the gyp24 curve occurs in both **b** and **c**. To the right, experimental conditions of the tests are shown in pressure–temperature space in relation to equilibrium conditions established for bassanite: *continuous line* corresponds to calculated equilibrium gypsum to bassanite-α* and water using thermodynamic data available (see Supplementary Tables 1, 2 and Supplementary Figs. 1, 2). *Black dots* represent P_c and unfilled circles P_f in the experiments

Results

Volumometry

Thirty five experiments were run over a range of temperature, confining pressure and fluid pressure. In many experiments, we *controlled* the fluid pressure at the top of the sample but just *monitored* it at the base, where it would build up from the initial value unless fluid could escape through the specimen. In some cases, transient pressure increases are seen at the base, but later sufficient porosity is generated by the reaction to allow fluid escape (Ko et al. 1995; Ko et al. 1997). In this configuration, all fluid flow must be towards the drained end—this reflects fluid pressure gradients; hence, fluid pressure must decrease monotonically from undrained to drained end. Therefore, if fluid pressures at top and bottom are roughly equal, we expect the fluid pressure field to be close to uniform throughout (this is in contrast to having *both* ends drained, in which case there could be a fluid pressure maximum at the sample midpoint). Hence, to an adequate approximation, the fluid volume expelled reflects the combined reaction and compaction rate—there is no "hidden" fluid in impermeable, over pressured regions (Tenthorey and Cox 2003).

Figure 4 illustrates selected experiments allowing visualization of the relative effects of three parameters: (a) temperature, (b) pore fluid pressure, and (c and d) confining pressure. In Fig. 4a–c, we have adjusted the volume expelled by dividing it by the volume expelled when expulsion rate is at a maximum. Consequently, each curve has a maximum gradient when the adjusted volume is 1. Figure 4d is the normalized expelled volume with respect to sample volume but unadjusted to maximum expulsion rate. Comparing it with Fig. 4c shows that the confining pressure has a strong effect on the amount of water expelled, but not on the overall timescale over which that expulsion occurs.

A series of separate experiments with pore fluid pressures of 90, 40 and 10 MPa (Fig. 4b) shows a significant increase in reaction rates with decreasing pore fluid pressure from conditions, where $P_c = P_f$ to extreme conditions where $P_c \gg P_f$. A group with confining pressures of 15, 50 and 110 MPa in separate experiments (Fig. 4c, d) show that the confining pressure has a limited effect on the overall reaction rates. Compare Fig. 4b and c, noting the shorter time axis in Fig. 4c.

The entire dataset of 35 experiments (Supplementary Table 3) is displayed in Figs. 5 and 6. In Fig. 5, log of reaction rate proxy for every experiment is plotted against free energies calculated first using the pressure of the fluid (black circles), then confining pressure (grey circles). When using pore fluid pressure, a stronger correlation between reaction rate and free energy is observed, compared to when confining pressure is used. It should be noted

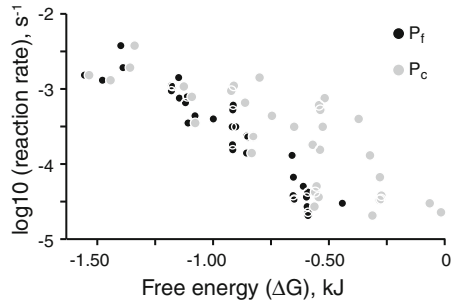

Fig. 5 Free energy of reaction calculated for a situation where all phases are under hydrostatic pressure P_f (*black dots*) or P_c (*grey dots*), plotted against reaction rate proxy

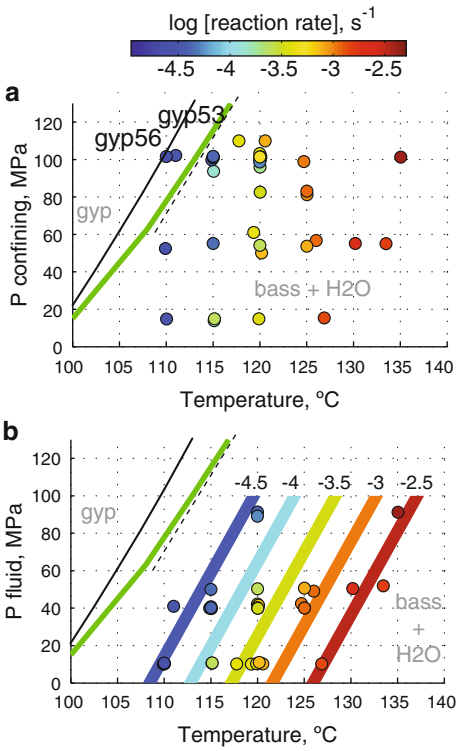

Fig. 6 *Colour-coded* reaction rates, adjusted for compaction. **a** Variation with temperature and confining pressure. **b** Variation with temperature and pore fluid pressure, together with "contours" of reaction rate derived from the linear regression. The "contours" are in fact strips, the width of the strip representing the influence of varying confining pressure from 10 to 100 MPa. The *graphs* illustrate that the effect of the confining pressure on rates (**a**) is substantially less than of pore fluid pressure (**b**). The scale for log of reaction rate proxy is shown in the *colour bar* at the top of the graphs. *Equilibrium lines* in the background are similar to those in Fig. 4

that in all graphs, the use of reaction rate proxy markedly reduces the scatter in the rate data, compared to using the maximum expulsion rate.

The plot calculated using P_c does show *some* correlation but we now demonstrate that this is mainly due to the dependence of $\Delta_r G^\circ$ on temperature. In Fig. 6, all

experiments are presented in a pressure–temperature graph, where reaction rate proxy is colour-coded as a function of P_c (Fig. 6a) and P_f (Fig. 6b). The temperature dependence is obvious, as is a pattern of lower reaction rates at elevated P_f, but there is little influence of P_c on the reaction rate. The data were linearly regressed to gain more insight into the relative effects of the three controlling parameters, the outcome being

$$\log_{10}(\text{rate proxy}) = -16.9851 + 0.1142\,T - 0.0127\,P_f + 0.0019\,P_c \quad (7)$$

This confirms quantitatively that there is a much stronger dependence on pore fluid pressure than on confining pressure with the P_f coefficient being six times larger. Equally important, though, is the different sign. The negative P_f coefficient is entirely in accord with the positive slope of the reaction line: as P increases, there is a smaller driving force for reaction as we are closer to the equilibrium line. The 95% confidence limits for this coefficient are -0.0170 to -0.0085. P_c appears to slightly *enhance* reaction rate; however, the confidence limits for this coefficient are -0.0008 to 0.0046. It is premature, then, to claim any dependence of reaction rate on P_c. Figure 6b shows "contours" of reaction rate as a backdrop to original reaction rate data. Each contour is a strip of finite width covering a range of P_c values from 10 to 100 MPa. The narrowness of these strips is a visual indication of the insensitivity of reaction rate to P_c. The strips have similar slopes to the reaction line because the reaction rate is a function dominated by the effect of $\Delta_r G^\circ$.

Microstructure

The product microstructures are complicated, as bassanite occurs in 3 different morphologies and commonly in aggregates rather than being uniformly dispersed (Hildyard et al. 2011). For the purpose of this contribution, we would ideally like to see at which points the bassanite and porosity were developing, and at which points the gypsum was dissolving but this is not straightforward to establish (see Fusseis et al. 2011).

The elongate bassanite morphology results from fastest growth at the ends of the needles. For long needles, these ends are often truncated during the making of the thin section (e.g., gyp38, Fig. 7a, b). For shorter needles, the ends are defined by multiple slender terminations (e.g., gyp22, Fig. 7c), with details too small to be resolved optically. Bassanite needles commonly crosscut gypsum grain boundaries. We know that bassanite needle orientation may be controlled by prior gypsum orientation (Hildyard et al. 2011) but this relates to nucleation; it does not necessarily give information on growth processes. The gypsum, visible where reaction is incomplete, shows undulose extinction. Pores do not show any particular pattern in their occurrence and are most evident in those samples deformed at low P_e where compaction has not occurred (e.g., Fusseis et al. 2011).

The delicate bassanite needles preserved, unbent, in both uncompacted and compacted samples imply that bassanite did not take up compactional strain. It is difficult even to envisage grain boundary sliding in such interlocking aggregates of needles as seen, for example, in gyp64 (Fig. 7d). Bassanite is stronger than gypsum and may also have "reinforced" areas of gypsum in which it grew. This is relevant for understanding the compaction, but the microstructures do not give extensive insight into reaction mechanism.

Discussion and summary

In the introduction, we stated that the chemical potentials are governed by the normal stresses at solid surfaces and interfaces. Each of the pathways will have different local chemical potentials associated with it. For example in Path 4 (Fig. 1a), the chemical potential of gypsum is determined by σ_s where it dissolves, whilst the chemical potential of precipitating bassanite is determined by P_f. Since σ_s–P_c, we would expect some influence of P_c on reaction rate. The only path we have illustrated where P_c does not significantly affect chemical potentials is Path 1. This suggests that gypsum is dissolving into, and bassanite growing primarily from, the porosity generated by the reaction. This was proposed for serpentinite dehydration by Llana-Fúnez et al. (2007). In their experiments, the matrix did not compact significantly, and hence it is reasonable to argue that the reaction products were not supporting the confining pressure. In Rutter et al. (2009), only part of the reaction products, forsterite grains forming in honeycomb pattern, were bearing the confining pressure when dehydration occurred under effective pressure. Our experiments provide new insight because the matrix is compacting, thereby maintaining relative high values of contact area between grains (paths 2 and 4 in Fig. 1a). At all stages of growth, bassanite will be in contact with gypsum or other bassanite grains and must be supporting some of the confining pressure. Remarkably, though, even when the specimen contains substantial bassanite, the increased normal stresses that the bassanite grains must be supporting along solid/solid contacts do not seem to inhibit their growth. Experiment gyp56 is the most extreme example; here, the reaction proceeded apace, even though the confining pressure was so high that a solid interface under that normal stress would almost favour gypsum not bassanite (Fig. 6a).

Ideally, the microstructures we document would provide information on sites of bassanite formation, but in practice,

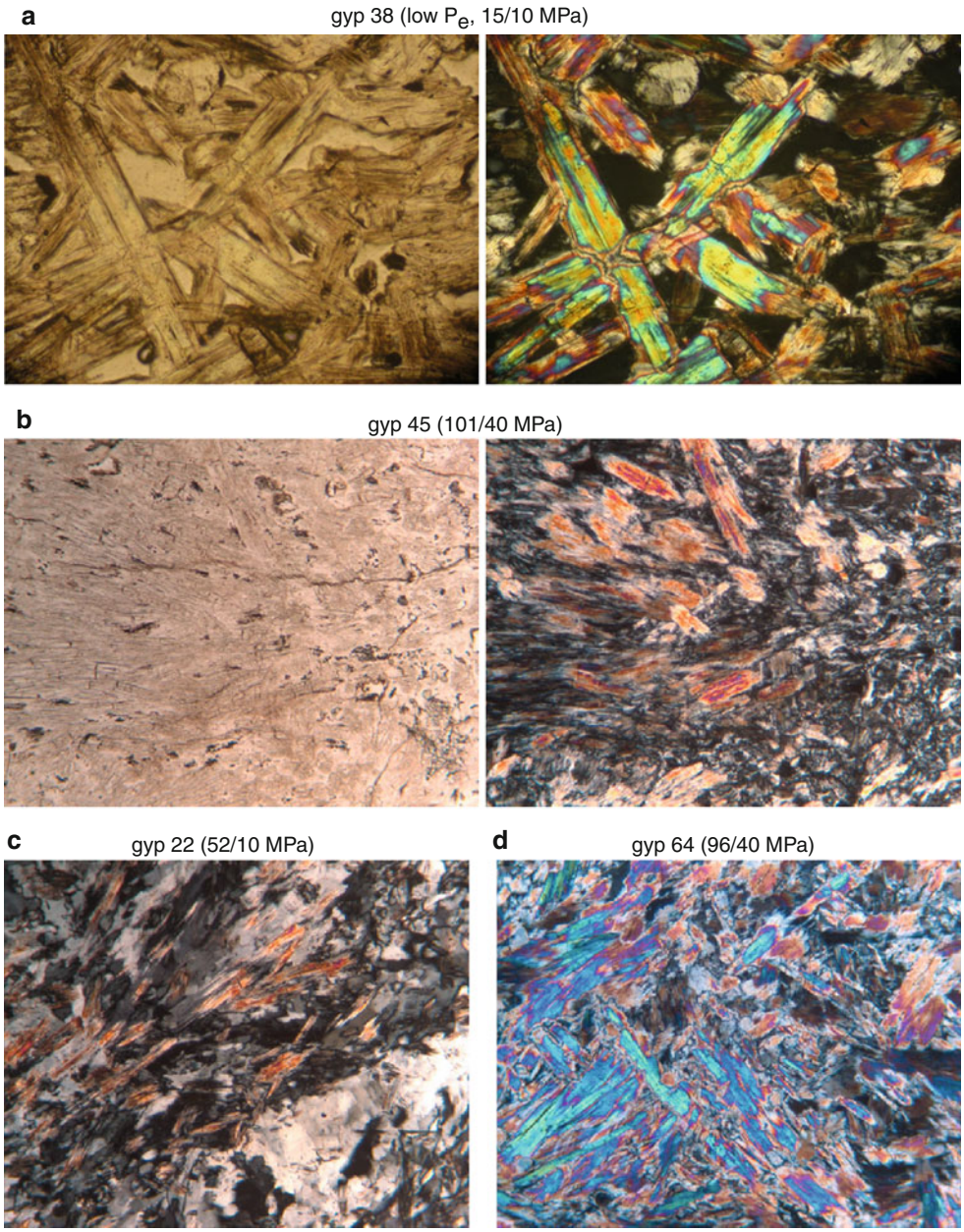

Fig. 7 Plane and cross-polarized light photomicrographs of selected experimental products: gypsum shows just grey interference colours, bassanite up to first-order *blue*. **a** Gyp38: note prominent pores between bassanite laths. **b** Gyp45: "cloudy" bassanite (Hildyard et al. 2011); some minor pores outlined by polishing powder lodged during preparation. **c** Gyp22: delicate bassanite laths within gypsum. **d** Gyp64: interlocking bassanite laths

they are ambiguous (section "Microstructure"). This underlines the importance of our experimental studies. Perhaps reactions are accompanied by small or transient pores, which have not been observed in final microstructures but which nevertheless sustain particular transport pathways.

We have no reason to suppose that gypsum behaviour is *fundamentally* different to that of other hydrous minerals. We therefore suggest that the dominant effect of pore fluid pressure over the reaction progress will be a general feature of dehydration and devolatilization reactions, with the timescales over which it applies being a function of several linked kinetic parameters.

There are several situations where this is important. First, rapid changes in fluid pressure are expected after earthquakes (Sibson et al. 1988; Sibson 2004). Even if lithostatic pressure stays approximately fixed, a reduction in pore fluid pressure through dilatancy will promote reaction (Miller et al. 2003), which may affect how the earthquake propagates and also how aftershocks develop. Second, in basins undergoing diagenesis and metamorphism, the results of our experimental work suggest that the reactions will be governed by the pore fluid pressure. Consequently, any overpressure may suppress reactions. Third, during mineralization, fluids flow through rocks and interact chemically. The existence of fluid pathways means

that the fluid pressure field will likely be different to the lithostatic pressure. Our results show that the fluid pressure will control reactions. Previous work has made such an assumption but lacked tests (Dahlen 1992) or theoretical justification. Bruton and Helgeson (1983) worked on the assumption that all equilibria would be dominated by solid–fluid interfaces, though they were aware that solid–solid interfaces support different normal stresses and lead to different local equilibria.

Finally, although our experiments cover a variety of conditions, they were conducted over short timescales. Some documented phenomena *do* indicate the influence of confining pressure on chemical processes, namely compaction by pressure solution. This has been described for powdered high-porosity gypsum synthetic aggregates (de Meer and Spiers 1995). The underlying theory makes clear that the process is driven by chemical potential differences between solid–solid contacts and solid–fluid contacts. These differences drive diffusive fluxes out of solid–solid contacts and into pores where gypsum reprecipitates (similar to Path 4 on Fig. 1a), allowing grains to become closer together and compaction to occur. It may be that the different timescales of this particular compaction process and of our studied reaction have influenced different levels of chemical communication within the grain boundary—pore network. Further work is required to explore this idea, and we suggest that fundamental insights will be gained by investigating the spatial and temporal overlaps between reaction and pressure solution processes.

Acknowledgments This research was funded by NERC grant NE/C002938/1. SLF acknowledges funding from Subprograma Ramón y Cajal (Ministerio de Ciencia e Innovación) RYC-2008-02067 during the writing of this paper. Earlier version of the manuscript benefited from constructive reviews by Stephen Cox and Bruce Yardley. For the new version, authors need to thank the feedback given by Tenfong Wong and the editor, Jon Blundy.

References

Ague JJ, Park J, Rye DM (1998) Regional metamorphic dehydration and seismic hazard. Geophys Res Lett 25(22):4221–4224

Bear J, Bachmat Y (1991) Introduction to modelling of transport phenomena in porous media. Kluwer, London

Bruton CJ, Helgeson HC (1983) Calculation of the chemical and thermodynamic consequences of differences between fluid and geostatic pressure in hydrothermal systems. Am J Sci 283A: 540–588

Dahlen FA (1992) Metamorphism of nonhydrostatically stressed rocks. Am J Sci 292(3):184–198

de Meer S, Spiers CJ (1995) Creep of wet gypsum aggregates under hydrostatic loading conditions. Tectonophysics 245(3–4):171–183

Fusseis F, Schrank C, Liu J, Karrech A, Llana-Fúnez S, Xiao X, Regenauer-Lieb K (2011) Unravelling gypsum dehydration by combining 4-dimensional Synchrotron tomography and thermodynamic models. Solid Earth Discuss 3:857–900

Fyfe WS, Price NJ, Thompson AB (1978) Fluids in the earth's crust: their significance in metamorphic, tectonic and chemical transport processes. Elsevier Scientific Pub. Co.: distributions for the U.S. and Canada Elsevier/North-Holland, Amsterdam, New York

Hanshaw BB, Bredehoeft JD (1968) On maintenance of anomalous fluid pressures: II. Source layer at depth. Geol Soc Am Bull 79(9):1107–1122

Heard HC, Rubey WW (1966) Tectonic implications of gypsum dehydration. Geol Soc Am Bull 77(7):741–760

Hildyard RC, Prior DJ, Mariani E, Faulkner DR (2009) Crystallographic preferred orientation (CPO) of gypsum measured by electron backscatter diffraction (EBSD). J Microsc Oxf 236(3): 159–164. doi:10.1111/j.1365-2818.2009.03292.x

Hildyard RC, Llana-Fúnez S, Wheeler J, Faulkner DR, Prior DJ (2011) Electron backscatter diffraction (EBSD) analysis of bassanite transformation textures and crystal structure produced from experimentally deformed and dehydrated gypsum. J Petrol 52(5):839–856

Holland TJB, Powell R (1998) An internally consistent thermodynamic data set for phases of petrological interest. J Metamorph Geol 16(3):309–343

Kelley KK, Southard JC, Anderson CT (1941) Thermodynamic properties of gypsum and its dehydration products. Bureau of mines technical paper, US Department of Interior 625:1–73

Ko SC, Olgaard DL, Briegel U (1995) The transition from weakening to strengthening in dehydrating gypsum—evolution of excess pore pressures. Geophys Res Lett 22(9):1009–1012

Ko SC, Olgaard DL, Wong TF (1997) Generation and maintenance of pore pressure excess in a dehydrating system 1. Experimental and microstructural observations. J Geophys Res Solid Earth 102(B1):825–839

Lasaga AC (1997) Kinetic theory in the earth sciences. Princeton University Press, Princeton

Llana-Fúnez S, Brodie KH, Rutter EH, Arkwright JC (2007) Experimental dehydration kinetics of serpentinite using pore volumometry. J Metamorph Geol 25:423–438

McConnell JDC, Astill DM, Hall PL (1987) The pressure-dependence of the dehydration of gypsum to bassanite. Mineral Mag 51(361):453–457

Miller SA, van der Zee W, Olgaard DL, Connolly JAD (2003) A fluid-pressure feedback model of dehydration reactions: experiments, modelling, and application to subduction zones. Tectonophysics 370(1–4):241–251

Milsch HH, Scholz CH (2005) Dehydration-induced weakening and fault slip in gypsum: Implications for the faulting process at intermediate depth in subduction zones. J Geophys Res Solid Earth 110(B4):1–16

Milsch H, Priegnitz M, Blöcher G (2011) Permeability of gypsum samples dehydrated in air. Geophys Res Lett 38:6

Mirwald PW (2008) Experimental study of the dehydration reactions gypsum-bassanite and bassanite-anhydrite at high pressure: Indication of anomalous behavior of H2O at high pressure in the temperature range of 50–300 degrees C. J Chem Phys 128(7). doi:10.1063/1.2826321

Mitchell TM, Faulkner DR (2008) Experimental measurements of permeability evolution during triaxial compression of initially intact crystalline rocks and implications for fluid flow in fault zones. J Geophys Res Solid Earth 113(B11). doi:10.1029/2008jb005588

Olgaard DL, Ko SC, Wong TF (1995) Deformation and pore pressure in dehydrating gypsum under transiently drained conditions. Tectonophysics 245(3/4):237–248

Partridge EP, White AH (1929) The solubility of calcium sulfate from 0 to 200°C. J Am Chem Soc 51:360–370

Paterson MS (1973) Nonhydrostatic thermodynamics and its geologic applications. Rev Geophys Space Phys 11(2):355–389

Posjnak E (1938) The system $CaSO_4$-H_2O. Am J Sci 35A:247–272

Rubie DC, Thompson AB (1985) Kinetics of metamorphic reactions at elevated temperatures and pressures: an appraisal of available experimental data. In: Thompson AB, Rubie DC (eds) Metamorphic reaction kinetics, textures, and deformation, vol. Springer, Berlin, pp 27–79

Rutter EH, Llana-Fúnez S, Brodie KH (2009) Dehydration and deformation of intact cylinders of serpentinite. J Struct Geol 31(1):29–43. doi:10.1016/J.Jsg.2008.09.008

Sibson RH (2004) Controls on maximum fluid overpressure defining conditions for mesozonal mineralisation. J Struct Geol 26(6–7):1127–1136. doi:10.1016/j.jsg.2003.11.003

Sibson RH, Robert F, Poulsen KH (1988) High-angle reverse faults, fluid-pressure cycling, and mesothermal gold-quartz deposits. Geology 16(6):551–555

Stretton I (1996) An experimental investigation of the deformation properties of gypsum. PhD, University of Manchester

Stretton IC, Schofield PF, Hull S, Knight KS (1997) The static compressibility of gypsum. Geophys Res Lett 24(10):1267–1270

Tenthorey E, Cox SF (2003) Reaction-enhanced permeability during serpentinite dehydration. Geology 31(10):921–924

Wang WH, Wong TF (2003) Effects of reaction kinetics and fluid drainage on the development of pore pressure excess in a dehydrating system. Tectonophysics 370(1–4):227–239

Wheeler J (1987) The significance of grain-scale stresses in the kinetics of metamorphism. Contrib Mineral Petrol 97(3):397–404

Wong TF, Ko SC, Olgaard DL (1997) Generation and maintenance of pore pressure excess in a dehydrating system. 2. Theoretical analysis. J Geophys Res Solid Earth 102(B1):841–852

Yamamoto H, Kennedy GC (1969) Stability relations in system $CASO_4$–H_2O at high temperatures and pressures. Am J Sci 267:550–557

Zen EA (1965) Solubility Measurements In System $Caso_4$–NaCl–H_2O At 35°, 50°, And 70°C and one atmosphere Pressure. J Petrol 6(1):124–164